RSC Advances

ROYAL SOCIETY OF CHEMISTRY

www.rsc.org/advances

Cite this: DOI: 10.1039/c0xx00000x

www.rsc.org/Advances

COMMUNICATION

Bifunctional gold-manganese oxide nanocomposites: Benign electrocatalysts towards water oxidation and oxygen reduction

Hasimur Rahaman, Koushik Barman, Sk Jasimuddin and Sujit Kumar Ghosh*

Received (in XXX, XXX) Xth XXXXXXXXX 20XX, Accepted Xth XXXXXXXXX 20XX

DOI: 10.1039/b000000x

Gold-manganese oxide nanocomposites have been synthesised by seed-mediated epitaxial growth at water/*n*-heptane interface under mild reflux condition. These nanocomposites exhibit efficient electrocatalytic activity towards water oxidation reaction (WOR) and simultaneous oxygen reduction reaction (ORR) at low overpotential (η≈ 370 mV) and neutral pH condition.

1. Introduction

Industrial scale production of clean energy could replace finite fossil fuels with abundant, renewable, environmentally benign energy sources and led to survive the planet in a sustainable way that poses a great challenge to humanity in the 21st century.[1,2] There is a growing need for electrocatalytic water oxidation to give dioxygen for the conversion of electrical energy to stored chemical energy in the form of fuels.[3,4] Plant life is bestowed upon complex catalytic systems for the disintegration of water into its elements; in natural and many protocols designed for artificial photosynthesis, water oxidation, $2H_2O \rightarrow 4H^+ + O_2 + 4e^-$, is a significant step and our understanding of these systems could pioneer in designing effective catalysts.[5,6] The activity of the electrocatalysts for water oxidation is of fundamental importance for the development of promising energy conversion technologies, including, integrated solar water-splitting devices, water electrolyzers, and lithium-air batteries.[7] Therefore, to meet the challenges that lie ahead, water oxidation has become thrust area of research materialistically inspired by the energy challenges and bio-inspired by the emerging understanding of photosystem II.[8,9] The salient features of technical impediment to such a reaction is the need for efficient and inexpensive electrocatalysts capable of oxidizing water to drive this energetically highly unfavorable reaction (ΔH° = 572 kJ/mol).[10] Several protocols have been adopted in the literature to design an efficient, inexpensive and robust electrocatalysts for water oxidation reaction based on metallic platinum,[11] various oxides and complexes of iridium,[12] ruthenium,[13] nickel,[14] cobalt[15] and iron[16] and copper complexes[17] and to evaluate the oxygen evolution activity in acidic and/or alkaline conditions However, amongst the materials considered, so far, for water oxidation catalysts, first row transition metal oxides can offer high earth abundance and reasonable stability in comparison with their noble metal analogues.[18]

Manganese oxides are materials of considerable importance due to their interesting structural, magnetic and transport properties that arise from their outstanding structural flexibility combined with novel chemical and physical properties.[19] Among the series of manganese oxides available in various oxidation states of manganese (II, III, IV), Mn_3O_4 (hausmannite) has been found to be an effective and inexpensive catalyst in a number of oxidation and reduction reactions.[20] On the otherhand, gold nanoparticles have attracted increasing attention due to their unique properties, such as, high biocompatibility, tunable electronic and optical behaviour, good conductivity and high catalytic activity, which make them fundamental building blocks for the development of innovative functional materials.[21] The assembly of different nanomaterials with specific optical, magnetic, or electronic properties to multicomponent composites can change and even enhance the properties of the individual constituents.[22] The bifunctional composite nanostructures containing gold have found tremendous importance in the field of nanocatalysis due to rich surface chemistry of gold.[23] The fabrication of nanocomposites containing two or more different functionalities has begun to garner attention for enhanced catalytic properties.[24]

Several reports have been published in the literature using manganese oxides and complexes as electrocatalysts for water oxidation. Dismukes et al.[25] have described the thermodynamic and mechanistic aspects that Nature appears to use to catalyze *in-vitro* water oxidation by photosynthesis using bioinspired and photoactive Mn_4O_4-cubane clusters. Drawing inspiration form these cubane-like CaMn(4)O(x), the biological catalyst found in the oxygen evolving centre in photosystem II, Gorlin and Jaramillo[26] have investigated the electrocatalytic activity of nanostructured manganese oxide surfaces that exhibited similar oxygen electrode activity to the best known precious metal nanoparticle catalysts, *viz.*, platinum, ruthenium and iridium. In a recent communication, Jaramillo and colleagues[27] have demonstrated that addition of Au to MnO_x produces an order of

Department of Chemistry, Assam University, Silchar-788011, India

Fax: +91-3842-270802; Tel: +91-3842-270848; E-mail: sujit.kumar.ghosh@aus.ac.in

magnitude higher turnover frequency than that of the best pure MnO_x catalysts and a local rather than bulk interaction between Au and MnO_x leads to the observed enhancement in the activity of the reaction. Zaharieva and co-authors[28] have shown that a binuclear manganese molecular complex $[(OH_2)(terpy)Mn(\mu\text{-}O)_2Mn(terpy)(OH_2)]^{3+}$ which is the most prominent structural and functional model of the water-oxidizing manganese complexes operating in plants and cyanobacteria, could be supported on montmorillonite clay and using Ce(IV) as a chemical oxidant, the complex could act as one of the best manganese-based molecular catalyst towards water oxidation. Wiechen et al.[29] have reported the syntheses of layered manganese oxides where the interlayer cations, *viz.*, K-, Ca-, Sr- and Mg-containing birnessites was varied and observed that oxygen-evolving complex require the presence of calcium in their structures to reach maximum catalytic activity. Spiccia and group[30] have shown that for the nanoparticulates of manganese oxides, formed in Nafion polymer, the catalytic activity towards the water oxidation is dependent on the dispersity of the nanoparticles. They have also reported that the synthetic methodologies for the preparation of highly active mixed valent MnO_x catalysts by partial oxidation of crystalline $Mn^{II}O$ nanoparticles and analysed the catalytic activity in water splitting devices.[31] In a review, the group have elucidated the perspectives of a cluster that contains four manganese and one calcium ions bridged by five oxygen atoms in a distorted chair-like arrangement in the current structural and mechanistic understanding of the oxygen evolving complex in photosystem II.[32] Being inspired by the structural diversity of manganese oxides that occur naturally as minerals in at least 30 different crystal structures, Dismukes and colleagues[33] have chosen to, systematically, compare eight synthetic oxide structures containing Mn(III) and Mn(IV) with cubic phases and concluded that electronically degenerate Mn(III) imparts lattice distortions due to the Jahn–Teller effect that are hypothesized to contribute to structural flexibility important for catalytic turnover in water oxidation at the surface. Suib and group[34] have compared the catalytic activity of mixed valent porous amorphous manganese oxides, cryptomelane-type tunnel manganese oxides and layered birnessite as water oxidation catalysts and observed that amorphous manganese oxides exhibit, significantly, higher turnovers compared to tunnel and layered structures. In spite of all these investigations with molecular and solid-state electrocatalysts, capable of mediating water oxidation, many fundamental questions and practical challenges remain, and improvements are needed in cost, durability and overpotential. In this communication, we have explored the controllable integration into gold-manganese oxide nanocomposites by seed-mediated epitaxial growth at water/*n*-heptane interface and investigated the electrocatalytic activity of the combinatorial catalysts towards water oxidation and oxygen reduction at low overpotential (370 mV) and the, most importantly, under neutral pH condition.

2. Experimental section

2.1 Reagents and instruments

All the reagents used were of analytical reagent grade. Gold(III) chloride trihydrate ($HAuCl_4.3H_2O$, ≥99.9%,), trisodium citrate (≥99%), manganese acetate tetrahydrate ($Mn(ac)_2.4H_2O$), 4-aminothiophenol (4-ATP), phosphoric acid were obtained from Sigma Aldrich and were used as received. Sodium perchlorate, sodium hydroxide, methanol, n-heptane and ammonia were purchased obtained from Sisco Research Laboratories, India and were used without further purification. An aliquot of 0.1 M phosphate buffer saline (PBS) was prepared by mixing of equimolar solution of phosphoric acid, and sodium perchlorate followed by dropwise addition of sodium hydroxide. Double distilled water was used throughout the course of the investigation. The temperature was 298±1 K for all experiments.

Absorption spectra were recorded in a Shimadzu UV-1601 digital spectrophotometer (Shimadzu, Japan) taking the sample in 1 cm well-stoppered quartz cuvette. Transmission electron microscopy (TEM) was carried out on a JEOL JEM-2100 microscope with a magnification of 200 kV. Samples were prepared by placing a drop of solution on a carbon coated copper grid and dried overnight under vacuum. Dark field scanning tunneling electron micrograph (DF-STEM) and selected area electron diffraction (SAED) pattern were obtained using the same instrument. Energy dispersive X-ray (EDX) analysis was performed on an INCA Energy TEM 200 using an X-ray detector. Fourier transform infrared (FTIR) spectra were recorded in the form of pressed KBr pallets in the range (400-4000 cm-1) in Shimadzu-FTIR Prestige-21 spectrophotometer. X-ray diffraction (XRD) pattern was obtained using a D8 ADVANCE BROKERaxs X-ray Diffractometer with CuK_α radiation (λ = 1.4506 Å); data were collected at a scan rate of 0.5° min-1 in the range of 10º-80º. Electrochemical measurements were performed by a CHI-660C electrochemical workstation. An Ag/AgCl electrode (in 3.0 M KCl) and a Pt wire were used as reference and auxiliary electrodes, respectively. Catalytic reactions were performed by the immobilized nanoparticles or nanocomposites over a 4-aminothiophenol monolayer modified gold working electrode where 0.1 M phosphate buffer saline (pH~7.5) was used as electrolyte and the scan rate was 100 mV/s.

2.2 Synthesis of the nanomaterials

2.2.1 Synthesis of gold nanoparticles (NPs)

Gold nanoparticleswere synthesised by Frens citrate reduction procedure.[35] A standard procedure for the preparation of 10 nm gold nanoparticles is as follows. An aliquot of 50 mL aqueous solution of $HAuCl_4.3H_2O$ (0.25 mM) is heated to boiling and 0.5 mL of trisodium citrate (1%) is added. In about 25 s, the boiling solution turns faintly blue (nucleation). After approximately 70 s, the blue colour suddenly changes into a brilliant red, indicating the formation of gold particles. The boiling was continued for half an hour and then cooled to room temperature.2.3 Synthesis of gold nanoparticles

2.2.2 Synthesis of gold-manganese oxide nanocomposites (NCs)

Gold-manganese oxide nanoparticles have been synthesised at environmentally benign water/*n*-heptane interface under mild reflux condition. In 25 mL binary solvent mixture of water and *n*-heptane (3:1 v/v), 2.5 mM $Mn(ac)_2.4H_2O$ was added and brought to reflux (*ca.* 65-70°C) under stirring. After about 30 min, 150 µL of ammonia was added and immediately after, 1.0 mL of

preformed gold nanoparticles (0.25 mM) was added dropwise continuing 10 min to the solution under reflux. The refluxing was continued overall for 1.5 h. After addition of the gold colloid, the colour of the sol was, slowly, begun to change and finally, a brownish red colouration was seen at the end of the reaction. Then, the heating was stopped and the mixture was stirred for 12 h at room temperature. The particles so obtained were retrieved from the solvent mixture by centrifugation at 10,000 rpm for 15 min and were, subsequently, redispersed into water. The dispersion was found to be stable for a month while stored in the vacuum desiccator. Manganese oxide nanoparticles were synthesised following the same procedure devoid of addition of any gold nanoparticles.the particles

3. Results and discussion

In the present experiment, water/*n*-heptane binary solvent mixture plays an important role in the evolution of gold-manganese oxide nanocomposites by epitaxial growth without any external stabilizing agents.[36] The controllable integration of gold and manganese oxide into single nanostructures has been characterised by absorption, Fourier transform infrared (FTIR) spectroscopy and X-ray diffraction (XRD) techniques, which reveal the epitaxial growth of manganese oxide on the surface of gold nanoparticles as described in ESI 2.

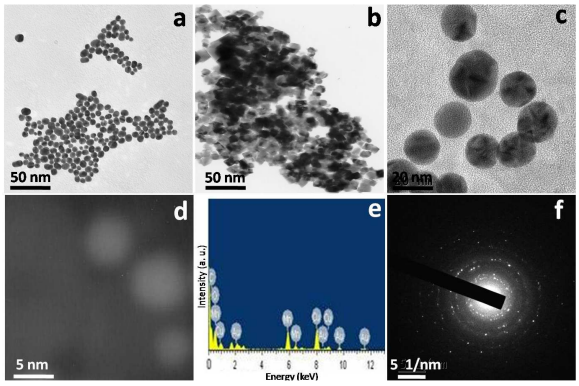

Fig. 1. (a, b, c) Transmission electron micrographs of Au, Mn_3O_4, and Au-Mn_3O_4 nanoparticles respectively; (d) dark field scanning tunneling electron micrographs, (e) energy dispersive X-ray, and (f) selected area electron diffraction pattern of Au.

The morphology, composition and crystallinity of the particles are depicted in Fig. 1. Ttransmission electron micrographs (panel a, b, c) of gold, manganese oxide, gold-manganese oxide show that the particles are of 10±2, 15±3 and 20±5 nm, respectively. In the image of the nanocomposites, the Au particles appear black and Mn_3O_4 are light coloured because Au has a higher electron density and allows fewer electrons to transmit.[19] Dark field scanning tunneling electron micrographs (DF-STEM) (panel d) points out the epitaxial growth of manganese oxide on gold nanoparticles. The energy dispersive X-ray spectrum (panel e) of Au-Mn_3O_4 particles reveals that the particles are composed of Mn, C, O, Cu and Au elements. Among those elements, the signals of Mn, O and Au result from the Mn_3O_4 and Au particles which form the product and the signals of C, O and Cu elements come from the precursor and the supporting TEM grid. From the SAED pattern of the composites, it is clear that a bright reflection appears from the (111) plane of fcc structured gold and a strong ring pattern corresponding to (101), (103) and (211) planes of tetragonal hausmannite structure. In addition, a combined multireflection results due to Au-Mn_3O_4 composite formation, confirming the crystallinity of the resultant materials.[19]

Now, Au, Mn_3O_4 and Au-Mn_3O_4 nanoparticles have been employed to investigate the electrocatalytic activity towards water oxidation reaction. A detailed procedure of the modification of the electrodes has been described in ESI 3.

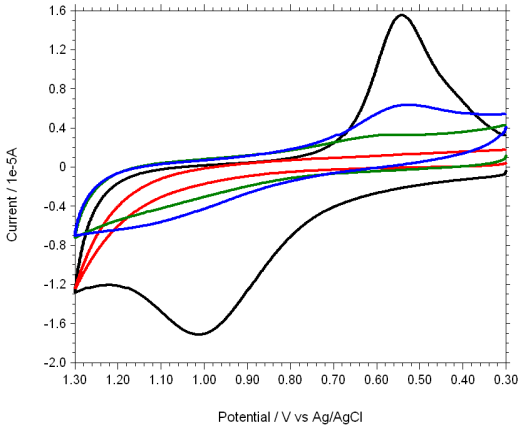

Fig. 2. Cyclic voltammograms of water oxidation in presence of 4-ATP/gold (red), Au NPs/4-ATP/gold (green), Mn_3O_4 NPs/4-ATP/gold (blue) and Au-Mn_3O_4 NCs/4-ATP/gold (black) electrodes in PBS at pH~7.5.

Fig. 2 displays the cyclic voltammogram of 4-ATP/gold (red), Au NPs/4-ATP/gold (green), Mn_3O_4 NPs/4-ATP/gold (blue) and Au-Mn_3O_4 NCs/4-ATP/gold (black) electrodes in PBS at pH~7.5. A particular amount (20 µg) of the catalysts was dissolved in 10 mL of water in each case. These dispersions were, then, employed for the loading of catalysts by dipping the electrodes and allowed to equilibrate overnight under vacuum. It is observed that Au-Mn_3O_4 nanocomposites (black) causes a shift of oxidation potential in the less positive potential and a large increase of current height compared to that of only Au (green) or Mn_3O_4 nanoparticles (blue). In spite of an ideal electrocatalytic process at its thermodynamic potential (for example, at 0.62 V *vs.* Ag/AgCl, pH ~7.0 and 1 atm O_2), the actual electrode reaction occurs at a more positive potential (i. e., overpotential) whose magnitude reflects the electrode kinetics of the solution. It is seen that Au NPs/4-ATP/gold, Mn_3O_4 NPs/4-ATP/gold and Au-Mn_3O_4 NCs/4-ATP/gold electrode displays anodic response at +1.13 V ($\eta \approx 0.51$ V, pH~7.5) , +1.12 V ($\eta \approx 0.50$ V, pH~7.5) and +0.998 V ($\eta \approx 0.37$ V, pH~7.5) *vs.* Ag/AgCl, respectively in the potential window 0.3 - 1.3 V signifying water oxidation in 0.1 M PBS (pH ~ 7.5) and the corresponding cathodic peak at ~ + 0.5 V for $O_2 + 4H^+ + 4e \rightarrow 2H_2O$ at the pH~7.5 indicative of the reversibility of the process,[3] whereas no such signal appeared for 4-ATP/gold electrode. It was noted that the particles synthesized, in the present experiment, are stable for a couple of weeks without any significant agglomeration or precipitation of the

particles. After the deposition of the particles at the electrodes, the catalytic activity of the particles was measured and the electrodes were rinsed in distilled water after the experiments. It was noted that the electrodes retain their catalytic activity even after 48 h of the loading of the catalysts. Therefore, it could be conceived that the particles do not suffer from dissolution or corrosion during the time of measurement of their electrocatalytic activity. However, assuming that the particles are nearly spherical and the density of Mn_3O_4 and Au-Mn_3O_4 as 4.86 and 12.09 g cm^{-3} (taking an average of the density of Au and Mn_3O_4) respectively, the number of Mn_3O_4 and Au-Mn_3O_4 particles is *ca.* 2.3 × 10^{12} and 3.8 × 10^{11} respectively and the corresponding surface area is *ca.* 1625 × 10^{12} and 477 × 10^{12} nm^2, respectively.[37] Therefore, it is evident that Au-Mn_3O_4 composites are better electrocatalysts than the Mn_3O_4 particles.

The turnover frequency (TOF) of the catalysts could be calculated using the equations[38]:

$$I_{cat} = nFAk_{cat}\Gamma_{cat} \quad (1)$$

$$\Gamma_{cat} = Q/nFA \quad (2)$$

where, I_{cat} is the catalytic current density, n the moles of electron transfer, F the Faraday constant, A the geometric surface area of the underlying anodic surface, k_{cat} the rate constant of the electron transfer, Γ the surface coverage in moles per square centimeter and Q the charge obtained by integrating the cathodic peak (= $\int i_f$ dt, where i_f is Faradaic current). However, the concept of turn-over frequency is based on the number of the active sites of the catalysts. In the above equations, the active sites have been replaced as surface area, which is an apparent value; therefore, the calculated TOFs provide only apparent values rather than the real TOFs of the catalysts. In addition, for the catalyst of Au-Mn_3O_4, the active sites for Au are different from that for Mn_3O_4 and as a result, the calculated TOF is a hybrid or average of that of the constituent particles. From eqn. (1) and (2), we can estimate the electroactive site turnover rate during O_2 evolution as,

$$k_{cat} = I_{cat}/Q \quad (3)$$

The catalytic current density for Au, Mn_3O_4 and Au-Mn_3O_4 is 3.8, 5.8 and 17.4 μA, respectively and the charge obtained by integrating the cathodic peak for Au, Mn_3O_4 and Au-Mn_3O_4 is 2.4, 2.6 and 3.8 μC, respectively. Therefore, the turn-over frequency corresponding to Au, Mn_3O_4 and Au-Mn_3O_4 is *ca.* 1.6, 2.2, and 4.6 s^{-1}, respectively. The catalytic activity for water oxidation was perceived for Au-Mn_3O_4 nanocomposites as compared to their individual counterparts as those not only combine the properties of both noble metal and metal oxides, but also bring unique collective and synergistic effect in comparison with single component materials.[27,39]

A variation of the gold particle size in the nanocomposites shows that the catalytic activity increases with decrease in particle size of the nanocomposites (ESI 4); this study elicites the reproducibile electrocatalytic activity of the nanocomposites. Therefore, it could be conceived that Au-Mn_3O_4 composites are more efficient catalysts for water oxidation reaction than the individual Au or Mn_3O_4 nanoparticles. The enhanced catalytic activity of the Au-Mn_3O_4 catalysts could be attributed to the beneficial presence of higher amount of oxidisable gold species and surface oxygen vacancies resulting from the strong interaction between Au and the reactive surface of Mn_3O_4 nanoparticles.[40] An increase in 5d vacancy of Au increases the interaction of O_2 and Au, thereby, enhancing the catalytic activity of Au in the composites.[41] However, interestingly, it was noted while the electrode was cycled to cathodic potential after several

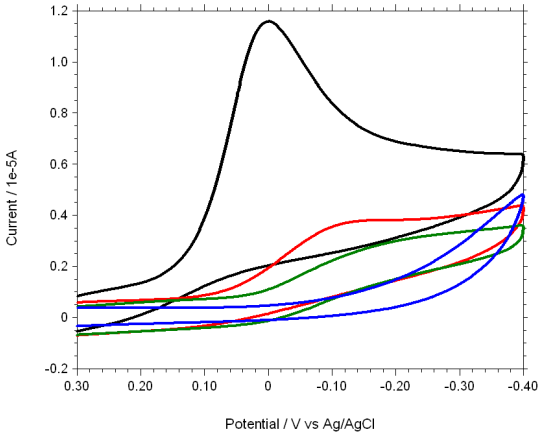

Fig. 3. Cyclic voltammograms for oxygen reduction in the presence of 4-ATP/gold (blue), Au NPs/4-ATP/gold (green), Mn_3O_4 NPs/4-ATP/gold (red) and Au-Mn_3O_4 NCs/ATP/gold (black) electrodes in PBS at pH~7.5.

scan through the catalytic anodic wave, an irreversible peak was observed at *ca.* - 0.001 to - 0.2 V for different modified electrode systems as presented in Fig. 3. This peak could be attributed to O_2/O_2^- couple[42] and indicates that O_2 was evolved from water oxidation on the electrode surface. A digital camera photograph showing the evolution of oxygen gas during water oxidation and the corresponding cyclic voltammogram of Au-Mn_3O_4 NCs/4-ATP/gold electrodes in normal and N_2-saturated PBS at pH~7.5 is shown in ESI 5. Under ambient condition the current height due to oxygen reduction is higher than N_2-sparged solution, which authenticates that the origin of this peak is originated due to O_2 reduction. In a like-wise manner of water oxidation, the higher cathodic peak current and lower reduction potential at Au-Mn_3O_4 NCs (black) than Mn_3O_4 NP (red) and Au NPs (green)-modified gold electrodes authenticate that the Au-Mn_3O_4 are better ORR catalysts than the individual Au or Mn_3O_4 particles.[37] The Au-Mn_3O_4 particles upon exposure to oxygen form radical species on the surface of the catalysts. The ability to form such radical species in the presence of oxygen leads to enhanced performance of the Au-Mn_3O_4 composites in the oxygen reduction reaction.[43] It is also likely that oxygen can dissociate on the Au surface and spill over from Au to the oxygen vacancies in the oxide, which synergistically promotes the adsorption and dissociation of O_2.[44] Therefore, the different surface structural features clearly determine the strength of metal-support interaction and thus the catalytic activity. The overpotential for Au, Mn_3O_4 and Au-Mn_3O_4 is 514, 505 and 370 mV, respectively. When Au interacts with transition metal oxides to form a reduced oxide and an oxidized metal at the interface of the two materials,[45,46] it dissolves at an oxidizing potentials relevant to the

Table 1. Cyclic voltammetry data of water oxidation and oxygen reduction in presence of nanomaterials

Catalysts	water oxidation potential ($E_{ox, H2O}$),V	I_{pa} # (μA)	1st oxygen reduction potential ($E_{red, O2}$), V	$I_{pc\ (1)}$ # (μA)	2nd oxygen reduction potential ($E_{red, O2}$), V	$I_{pc\ (2)}$ # (μA)
Au	1.134	-4.5	0.562 [50]	3.3	-0.189	2.9
Mn_3O_4	1.125	-6.8	0.515	6.3	-0.139	3.8
Au-Mn_3O_4	0.998	-17.1	0.546	15.6	-0.001	11.6

where, I_{pa} and I_{pc}denote the irreversible peak currents at anode and cathode, respectively.

water oxidation reaction.[47] Therefore, the presence of Au during the water oxidation reaction could lead to an enhancement in the electrocatalytic activity of Mn_3O_4 particles.

The oxidation of water to dioxygen is one of the key reactions that need to be fully understood in order to apply to water splitting devices. A reasonable mechanism for the water oxidation and oxygen reduction reactions on the nanocomposite surface could be enunciated as follows. From an electrochemical perspective, this reaction can be divided in two half reactions, water oxidation and proton reduction.[48] The formation of H_2O_2 from such species suggests that hydrolysis of an O–O bonded species proceeds more rapidly than the additional oxidation steps needed to form O_2. In the presence of the catalysts, an O–O bonded intermediate, can undergo rapid electron transfer in the material or to the electrode to enable selective evolution of O_2. In the present experiment, upon addition of gold to the metal oxide system, gold-metal oxide perimeter interface acts as a site for activating the reactants. Therefore, it could be conceived that very strong metal–support interactions after Au deposition,[49] creates a unique interface and that results in enhanced activity for water oxidation and oxygen reduction reactions.

Cyclic voltametry data of water oxidation and oxygen reduction in presence of the nanomaterials are summarized in Table 1. The overpotential of different manganese-based systems as a function of experimental conditions has been discussed elsewhere.[27] A comparative account of the pH condition of the experiment and overpotential of the Au-Mn_3O_4 and some other electrocatalysts is presented in ESI 6.

Fig. 4 illustrates the cyclic voltammograms at varying pH of the PBS with Au-Mn_3O_4 NCs/4-ATP/Au electrode. A little change of current height was observed for O_2/O_2^- couple at -0.18 V but the anodic peak potential as well as peak current varied with the change in pH of the solution (Fig. 4A). A plot of potential *vs.* pH and current *vs.* pH (Fig. 4B) show that the potential is optimum at pH~7.5 and the electrocatalytic activity for water oxidation increases with increasing pH (5.5 - 9.5) of the solution, respectively.

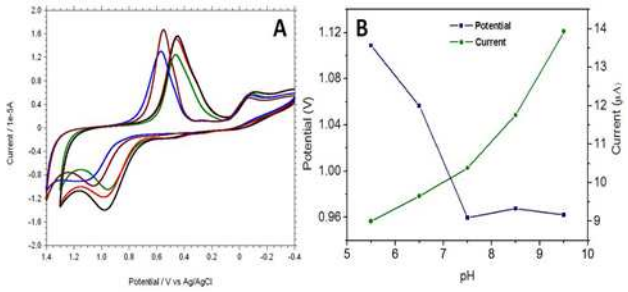

Fig. 4. (A) Cyclic voltammograms of water oxidation in 0.1 M PBS at pH~5.5 (blue), 6.5 (brown), 7.5 (green), 8.5 (red), 9.5 (black) with Au-Mn_3O_4 modified electrodes; and (B) Profile showing the variation of current and potential as a function of pH.

In conclusion, the synthesis of stabiliser-free gold-manganese oxide nanocomposites by seed-mediated epitaxial growth employing environmentally benign water/*n*-heptane interface paves a facile strategy through surface attachment for combinatorial catalyst design. We have, successfully, overcome the key challenge of recent research of electrocatalytic water oxidation, surprisingly, at nearly neutral pH (pH~7.5) and low overpotential of 370 mV which is beyond the typical range of many homogeneous water oxidation catalysts (600 – 900 mV). As manganese oxides are available in various oxidation states and exhibit extensive biomimetic chemistry with oxygen, this result adds a new feather and illuminates ample opportunities in water oxidation electrocatalysis using wide varieties of inexpensive and earth-abundant materials. This facile and environmentally benign synthetic strategy for the nanocomposites could be upscaled at the industrial level and may offer a promising future for renewable energy technologies.

Acknowledgement. We gratefully acknowledge financial support from DST, New Dehli (Project No.: SR/FT/CS-68/2010).

Supporting Information. Experimental details, cyclic voltammogram, digital camera images and reaction schemes. This material is available free of charge at http://www.rsc.org.

References

1. J. K. Hurst, *Science* 2010, **328**, 315–316.
2. S. Trassati, In The Electrochemistry of Novel Materials (Eds. J. Lipkowski, P. N. Ross) Wiley VCH, 1994, Ch. 5, pp. 207–296.
3. S. M. Barnett, K. I. Goldberg, J. M. Mayer, *Nature Chem.* 2012, **4**, 498-502.
4. R. Eisenberg, H. B. Gray, *Inorg. Chem.* 2008, **47**, 1697–1699.
5. J. H. Alstrum-Acevedo, M. K. Brennaman, J. T. Meyer, *Inorg. Chem.* 2005, **44**, 6802–6827.
6. F. Liu, J. J. Concepcion, J. W. Jurss, T. Cardolaccia, J. L. Templeton, J. T. Meyer, *Inorg. Chem.* 2008, **47**, 1727–1752.
7. M. G. Walter, E. L. Warren, J. R. McKone, S. W. Boettcher, Q. Mi, E. A. Santori, N. S. Lewis, *Chem. Rev.* 2010, **110**, 6443-6473.
8. N. S. Lewis, G. Crabtree, A. J. Nozik, M. R. Wasielewski, A. P. Alivisatos, Basic Research Needs for Solar Energy Utilization; Department of Energy, Washington, DC, 2005.
9. J. P. McEvoy, G. W. Brudvig, *Chem. Rev.* 2006, **106**, 4455–4483.
10. M. Grätzel, *Acc. Chem. Res.* 1981, **14**, 376-384.

11. N. S. Porter, H. Wu, Z. Quan, J. Fang, *Acc. Chem. Res.* 2013, **46**, 1867–1877.
12. T. Nakagawa, N. S. Bjorge, R. W. Murray, *J. Am. Chem. Soc.* 2009, **131**, 15578–15579.
13. L. Duan, F. Bozoglian, S. Mandal, B. Stewart, T. Privalov, A. Llobet, L. Sun, *Nature Chem.* 2012, **4**, 418–423.
14. M. J. Kenney, M. Gong, Y. Li, J. Z. Wu, J. Feng, M. Lanza, H. Dai, *Science* 2013, **342**, 836-840.
15. J. Z. McAlpin, T. A. Stich, C. A. Ohlin, Y. Surendranath, D. G. Nocera, W. H. Casey, R. D. Britt, *J. Am. Chem. Soc.* 2011, **133**, 15444–15452.
16. W. C. Ellis, N. D. McDaniel, S. Bernhard, T. J. Collins, *J. Am. Chem. Soc.* 2010, **132**, 10990–10991.
17. S. M. Barnett, K. I. Goldberg, J. M. Mayer, *Nature Chem.* 2012, **4**, 498–502.
18. N. S. Lewis, *Science* 2007, **315**, 798−801.
19. I. Djerdj, D. Arčon, Z. Jagličić, M. Niederberger, *J. Phys. Chem. C* 2007, **111***,* 3614-3623.
20. E. Grootendorst, Y. Verbeek, V. Ponce, *J. Catal.* 1995, **157**, 706–712.
21. C. -C. Hu, Y. -T. Wu, K. -H. Chang, *Chem. Mater.* 2008, **20**, 2890–2894.
22. S. K. Ghosh, J. Kang, M. Inokuchi, N. Toshima, *Appl. Catal. A* 2014, **464-465**, 225-232.
23. M. Haruta, *Faraday Discussions* 2011, **152**, 11–32.
24. *In* Metal Nanoclusters in Catalysis and Materials Science: The Issue of Size Control B. Corain*, G.* Schmid*, N.* Toshima*, Eds.* Elsevier, Amsterdam 2008.
25. G. C. Dismukes, R. Brimblecombe, G. A. N. Felton, R. S. Pryadun, J. E. Sheats, L. Spiccia, G. F. Swiegers, *Acc. Chem. Res.* 2009, **42**, 1935-1943.
26. Y. Gorlin, T. F. Jaramillo, *J. Am. Chem. Soc.* 2010, **132**, 13612–13614.
27. Y. Gorlin, C. –J. Chung, J. D. Benck, D. Nordlund, L. Seitz, T. –C. Weng, D. Sokaras, B. M. Clemens, T. F. Jaramillo, *J. Am. Chem. Soc.* 2013, **135**, 16977-16987.
28. M. M. Najafpour, A. N. Moghaddam, H. Dau, I. Zaharieva, *J. Am. Chem. Soc.* 2014, **136**, 7245–7248.
29. M. Wiechen, I. Zaharieva, H. Dau, P. Kurz *Chem. Sci.* 2012, **3**, 2330-2339.
30. A. Singh, R. K. Hocking, S. L. -Y. Chang, B. M. George, M. Fehr, K. Lips, A. Schnegg, L. Spiccia *Chem. Mater.* 2013, **25**, 1098–1108.
31. M. Wiechen, L. Spiccia, *Chem. Cat. Chem.* 2014, **6**, 439-441.
32. M. Wiechen, M. M. Najafpour, S. I. Allakhverdiev, L. Spiccia, *Energy Environ. Sci.* 2014, **7**, 2203-2212.
33. D. M. Robinson, Y. B. Go, M. Mui , G. Gardner, Z. Zhang, D. Mastrogiovanni, E. Garfunkel, J. Li, M. Greenblatt, G. C. Dismukes *J. Am. Chem. Soc.*, 2013, **135**, 3494–3501.
34. A. Iyer, J. Del-Pilar, C. K. King'ondu, E. Kissel, H. F. Garces, H. Huang, A. M. El-Sawy, P. K. Dutta, S. L. Suib *J. Phys. Chem. C* 2012, **116**, 6474–6483.
35. G. Frens, *Nature* 1973, **241**, 20-22.
36. M. Ali, S. K. Pal, H. Rahaman, S. K. Ghosh, *Soft Matter* 2014, **10**, 2767-2774.
37. Y. Tang, W. Cheng *Langmuir* 2013, **29**, 3125−3132.
38. T. Nakagawa, C. A. Beasley, R. W. Murray *J. Phys. Chem. C* 2009, **113**, 12959-12961.
39. G. Li, Z. Tang, *Nanoscale* 2014, **6**, 3995-4011.
40. F. W. Lytle, P. S. P. Wei, R. B. Greegor, G. H. Via, J. H. Sinfelt, *J. Chem. Phys.* 1979, **70**, 4849-4855.
41. A. L. Ankudinov, J. J. Rehr, J. J. Low, S. R. Bare, *J. Chem. Phys.* 2002, **116**, 1911-1919.
42. E. Yeager, *Electrochim. Acta* 1984, **29**, 1527-1537.
43. M. M. Schubert, S. Hackenberg, A. C. van Veen, M. Muhler, V. Plzak, R. J. Behm, *J. Catal.* 2001, **197**, 113–122.
44. L. M. Molina, B. Hammer, *Phys. Rev. Lett.* 2003, **90**, 206102 1–4.
45. J. D. Benck, Z. Chen, L. Y. Kuritzky, A. J. Forman, T. F. Jaramillo, *ACS Catal.* 2012, **2**, 1916−1923.
46. C. C. Chusuei, D. W. Goodman, *In* Encyclopedia of Physical Science and Technology; 3rd ed.; Robert, A. M., Ed.; Academic Press: New York, 2003, pp. 921−938.
47. V. M.-W. Huang, V. Vivier, M. E. Orazem, N. Pébère, B. Tribollet, *J. Electrochem. Soc.* 2007, **154**, C99−C107.
48. D. K. Zhong, D. R. Gamelin, *J. Am. Chem. Soc.* 2010, **132**, 4202–4207.
49. C. -C. Hu, Y. -T. Wu, K.-H. Chang, *Chem. Mater.* 2008, **20**, 2890–2894.

Table of Contents (TOC)

Bifunctional Au-Mn_3O_4 nanocomposites: Benign electrocatalysts towards water oxidation and oxygen reduction

Hasimur Rahaman, Koushik Barman, Sk Jasimuddin and Sujit Kumar Ghosh

G**old-manganese oxide nanocomposites** exhibit efficient **electrocatalytic activity towards water oxidation and oxygen reduction** at low overpotential and **neutral pH condition**.